Quantum electronic transport in semiconductors using the Wigner distribution from first principles

Andrea Cepellotti, and Boris Kozinsky
Harvard John A. Paulson School of Engineering and Applied Sciences,
Harvard University, Cambridge, MA 02138, USA

August 28, 2020

Abstract

Electronic transport properties of semiconductors with small band gaps are often not well described by semiclassical methods, because of missing interband interactions between carriers in the valence and conduction bands. We develop a new first-principles formalism based on the Wigner transform to generalize semiclassical transport models to include quantum effects. We apply the method to Bi_2Se_3, showing that bulk transport properties at low doping concentrations are dominated by the Zener effect, a mechanism in which carriers transfer charge by tunnelling across the band gap. Surprisingly, Zener tunneling occurs also between band subvalleys of energy much larger than the bandgap.

Recent years have seen the emergence of topological insulators (TI) as a new important class of materials, thanks to their variety of interesting physical properties and promising applications, such as low-power electronics and robust quantum bits [1, 2, 3, 4, 5]. Most studies focus on the surface states that result from the spin-orbit induced inversion of the bulk band gap, so that TIs behave as insulating crystals in the bulk, and as metals on surfaces. For applications in electronics, it is important to have a thorough understanding of both surface and bulk transport properties of TIs. In fact, several TIs are characterized by a bulk quasiparticle band gap that is much smaller than that of silicon. It is important to note that small band gap systems may behave differently than a silicon-based device. For example, small band gap graphene devices may display a phenomenon called Zener (or Klein) tunneling [6, 7], in which the tunneling of carriers through the band gap can substantially contribute to the electrical conductivity.

The de-facto tool of choice for first-principles simulation studies of electronic transport properties is the Boltzmann Transport Equation (BTE), which provides estimates of transport properties with remarkable agreement with experimental measurements (e.g. [8, 9, 10, 11, 12, 13]). However, this semiclassical approach is not always sufficient to model electronic transport properties: Zener tunneling, for example, is not captured. Some studies have used the equation of motion for the density matrix as an alternative description that holds for small band gap systems [14], however making difficult to understand the link with semiclassical models. Here instead we aim to extend the range of applicability of the BTE to complex materials, including narrow band-gap semiconductors such as Bi_2Se_3, with the benefit of retaining the capability to interpret the results in a simple fashion.

In this work, starting from the Moyal bracket, we derive an equation of motion for electrons, termed the Wigner transport equation (WTE). This equation allows the computation of the full set of electronic transport coefficients, and in particular the electrical conductivity and Seebeck coefficient, and reduces to the BTE in the limit where the Wigner function is diagonal. We implement this

equation with fully ab-initio parameters and apply the formalism to the topological insulator Bi_2Se_3. We show that at small doping concentrations, the estimates of bulk electronic transport properties deviate significantly from semiclassical estimates, due to the presence of Zener tunneling, which is instead captured by the WTE.

We start by considering the ground state Hamiltonian H_0 of a crystal, which we assume to be an independent-particle Hamiltonian with eigenvalues $\epsilon_b(\boldsymbol{k})$ and Bloch states $\psi_{\boldsymbol{k}b}(\boldsymbol{x})$, where $\boldsymbol{x}$ is the position, $\boldsymbol{k}$ the wavevector and b the band index (for simplicity, we omit the spin index). The ground-state is perturbed by a constant electric-field $\boldsymbol{E}$ which couples with the carriers' charge e and by the electron-phonon interaction H_{el-ph}, so that the total Hamiltonian is $H = H_0 + e\boldsymbol{x}\cdot\boldsymbol{E} + H_{el-ph}$. To derive an equation of motion for such a system, we use the single-particle Wigner function f of the system [15], defined as the Wigner transform of the density matrix ρ as

$$f_{bb'}(\boldsymbol{x},\boldsymbol{k},t) = \sum_{\Delta\boldsymbol{k}} e^{i\Delta\boldsymbol{k}\cdot\boldsymbol{x}} \rho_{bb'}\left(\boldsymbol{k}+\frac{\Delta\boldsymbol{k}}{2}, \boldsymbol{k}-\frac{\Delta\boldsymbol{k}}{2}; t\right) , \tag{1}$$

where t is the time. We build the Wigner function through a transformation of the density matrix $\rho_{bb'}(\boldsymbol{k},\boldsymbol{k}')$ in the reciprocal space representation. Such Wigner transform consists in a rotation of variables $\boldsymbol{k},\boldsymbol{k}' \rightarrow \frac{\boldsymbol{k}+\boldsymbol{k}'}{2}, \boldsymbol{k}'-\boldsymbol{k}$ combined with a Fourier transform on one variable. The Wigner function operates in a phase-space representation, which is especially useful to draw connections between quantum and classical mechanics.

The evolution of the Wigner function [16, 17] is found through a Wigner transform of the equation of motion of the density matrix, and has been shown to be

$$\frac{\partial f_{bb'}(\boldsymbol{x},\boldsymbol{k},t)}{\partial t} = -\left\{\left\{f(\boldsymbol{x},\boldsymbol{k},t), H(\boldsymbol{x},\boldsymbol{k})\right\}\right\}_{bb'} \tag{2}$$

$$:= \frac{i}{\hbar}\Big(f(\boldsymbol{x},\boldsymbol{k},t)\star H(\boldsymbol{x},\boldsymbol{k}) - H(\boldsymbol{x},\boldsymbol{k})\star f(\boldsymbol{x},\boldsymbol{k},t)\Big)_{bb'} , \tag{3}$$

where $\{\{f,H\}\}$ is the Moyal bracket (the quantum mechanical extension of the Poisson bracket) and the Moyal product $\star$ is defined as:

$$f\star H = f(\boldsymbol{x},\boldsymbol{k}) \exp\left(\frac{i}{2}\left(\frac{\overleftarrow{\partial}}{\partial\boldsymbol{x}}\cdot\frac{\vec{\partial}}{\partial\boldsymbol{k}} - \frac{\overleftarrow{\partial}}{\partial\boldsymbol{k}}\cdot\frac{\vec{\partial}}{\partial\boldsymbol{x}}\right)\right) H(\boldsymbol{x},\boldsymbol{k}) , \tag{4}$$

where $H(\boldsymbol{x},\boldsymbol{k})$ is the Wigner transform of the Hamiltonian, and the arrows indicate that the derivative operator is acting to the left/right operators. To ensure that such derivatives exist, we choose a particular wavefunction gauge, as discussed in the supplementary material.

We now simplify the Hamiltonian supposing that the electron-phonon interaction is weak and evaluate the Moyal bracket for the single-particle part of the Hamiltonian; the electron-phonon interaction is added later as a perturbation. Since we are interested in macroscopic properties, we can make the assumption that only slow spatial variations of the Wigner function are relevant. Therefore, we approximate the Moyal product in Taylor series to the lowest orders of $\hbar$ and, as detailed in the supplementary material, we find an equation of motion which we term the Wigner Transport Equation (WTE), that is

$$\frac{\partial f_{bb'}(\boldsymbol{x},\boldsymbol{k},t)}{\partial t} + \frac{i}{\hbar}\Big[\mathcal{E}(\boldsymbol{k}) + \boldsymbol{d}(\boldsymbol{k})\cdot\boldsymbol{E}, f(\boldsymbol{x},\boldsymbol{k},t)\Big]_{bb'} + \frac{1}{2}\Big\{\boldsymbol{v}(\boldsymbol{k}), \cdot\frac{\partial f(\boldsymbol{x},\boldsymbol{k},t)}{\partial\boldsymbol{x}}\Big\}_{bb'} - e\boldsymbol{E}\cdot\frac{\partial f_{bb'}(\boldsymbol{x},\boldsymbol{k},t)}{\partial\boldsymbol{k}} = -\left.\frac{\partial f_{bb'}(\boldsymbol{x},\boldsymbol{k},t)}{\partial t}\right|_{coll} . \tag{5}$$

where $\{,\}$ is an anticommutator, $\mathcal{E}_{bb'}(\boldsymbol{k}) = \delta_{bb'}\epsilon_{\boldsymbol{k}b}$ is a matrix of electronic energies, $\boldsymbol{d}_{bb'}(\boldsymbol{k}) = (1-\delta_{bb'})\langle \boldsymbol{k}b \,|\, e\boldsymbol{x} \,|\, \boldsymbol{k}b'\rangle$ is a matrix of electric dipoles between two Bloch states (typically used to describe optical excitations), and $\boldsymbol{v}_{bb'}(\boldsymbol{k})$ is the velocity operator. The electron-phonon scattering operator $\frac{\partial f_{bb'}(\boldsymbol{x},\boldsymbol{k},t)}{\partial t}\big|_{coll}$ is added as a perturbation to the WTE and is built, as detailed in the appendix, using scattering rates from the Fermi Golden rule [18, 19, 20, 21, 22].

The WTE must be solved to obtain the single-particle Wigner distribution function. As a first comment, we note that the BTE is recovered as a limiting case of the WTE, when the off-diagonal terms $b \neq b'$ are set to zero. This corresponds physically to a situation when different bands do not couple via Zener tunneling. This can happen, for example, when the energy difference is too large: if this is the case, neither thermal excitation nor dipole interaction provide sufficient energy to allow for the vertical transition of one particle from one band to another. Therefore, the most interesting terms to discuss in the WTE are the off-diagonal terms, which introduce the possibility of additional electronic transitions, or couplings, between different electronic states at a given wavevector $\boldsymbol{k}$. If we neglect the space derivative term, the WTE reduces to the quantum master equation studied in other works [23, 24, 25, 14, 26]; as discussed later, this additional term allows the computation of the Seebeck coefficient. Additionally, we note that the electronic WTE is conceptually similar to a formalism developed for phonon transport in Ref. [18], although here we use a simplified derivation and include the effect of external forces (the electric field).

To better understand the off-diagonal terms in Eq. 5, it is illustrative to estimate the electrical conductivity σ. The WTE can be solved to estimate σ with a technique similar to the one used to solve the BTE, and is detailed in the supplementary material. Once the Wigner distribution is known, transport properties are readily obtained. For example, the charge current density is

$$\boldsymbol{J} = \frac{e g_s}{2VN_k} \sum_{\boldsymbol{k}b} \Big\{ \boldsymbol{v}(\boldsymbol{k}), f(\boldsymbol{k}) \Big\}_{bb'} , \tag{6}$$

where g_s counts the spin degeneracy, V is the crystal unit cell volume and N_k counts the number of wavevectors. As detailed in the appendix, one can compute the electronic heat current as well, and thus the complete set of transport coefficients. The diagonal terms $b = b'$ correspond to the estimates of electrical conductivity tensor within the BTE formalism σ_{ij}^{BTE}, where i, j are cartesian labels. Notably, the semiclassical result is corrected by an additional term as $\sigma_{ij} = \sigma_{ij}^{BTE} + \Delta\sigma^{ij}$ with

$$\Delta\sigma^{ij} = \frac{2g_s e^2}{VN_k} \sum_{\substack{\boldsymbol{k}bb' \\ b\neq b'}} \frac{\bar{f}_{b'}(\boldsymbol{k}) - \bar{f}_b(\boldsymbol{k})}{\epsilon_{b'}(\boldsymbol{k}) - \epsilon_b(\boldsymbol{k})} \times \tag{7}$$

$$\times \frac{v^i_{bb'}(\boldsymbol{k}) v^{j,*}_{b'b}(\boldsymbol{k}) (\Gamma_b(\boldsymbol{k}) + \Gamma_{b'}(\boldsymbol{k}))}{4(\epsilon_{b'}(\boldsymbol{k}) - \epsilon_b(\boldsymbol{k}))^2 + (\Gamma_b(\boldsymbol{k}) + \Gamma_{b'}(\boldsymbol{k}))^2} ,$$

where $\Gamma_b(\boldsymbol{k})$ is the electronic linewidth (here, due to electron-phonon interaction) and $\bar{f}_b(\boldsymbol{k})$ the Fermi–Dirac occupation number. We can now make a few key remarks. First, the correction $\Delta\sigma$ is positive (note that $\bar{f}_b(\boldsymbol{k})$ is a monotonic function of $\epsilon_b(\boldsymbol{k})$), and therefore the WTE will always adjust the semiclassical prediction of conductivity to higher values. Second, the expression of the electrical conductivity better illustrates the role of the off-diagonal components of the Wigner distribution function. Whenever the energy difference between an electron and a hole is comparable to their linewidth, the two carriers interact. The strength of such interaction is determined by the velocity matrix element $v_{bb'}(\boldsymbol{k})$, i.e. the matrix element for optical transitions. As a result, the system allows an additional transport mechanism, known as Zener tunneling, in which electrons propagate by tunneling through the band gap.

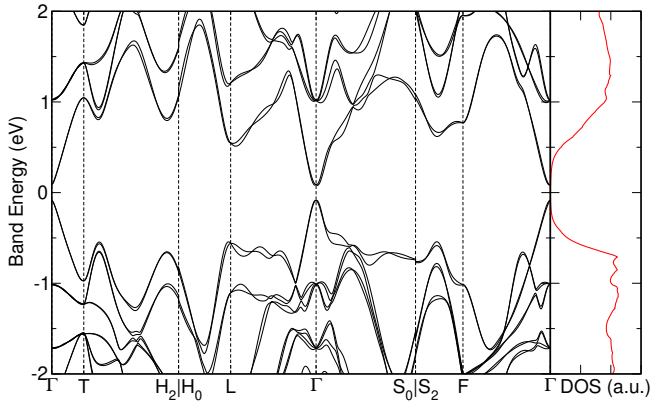

Figure 1: Electronic band structure and density of states (DOS) of Bi_2Se_3 near the Fermi energy, set at the center of the band gap. The bulk crystal is characterized by a small gap, opened by the spin-orbit coupling. We also note from the DOS that subvalleys of valence and conduction bands are approximately 1.8 eV apart in energy.

All quantities appearing in the WTE are available from first-principles codes and we can therefore apply this formalism using fully ab-initio parameters. In particular, we use Quantum ESPRESSO [27, 28] for the calculation of electronic and phonon properties [29], Wannier90 [30] to interpolate electronic energies and a mixed Wannier and linear interpolation of the electron-phonon matrix elements [12] (see Supplementary material for details).

We now apply the formalism to study the intrinsic lattice-limited electronic transport of bulk Bi_2Se_3. In Fig. 1 we report the band structure [31, 32] and the density of states (DOS) for this narrow-gap semiconductor. We estimate a quasiparticle gap of 0.2 eV, in agreement with experimental estimates [33]. It is worth noting that the DOS increases away from the Fermi level (set at 0 eV at the middle of the band gap) and flattens at energies of approximately -0.8eV and 1.0eV for the valence and conduction bands, respectively, indicating that the subvalleys are separated by an energy of approximately 1.8 eV.

In Fig. 2a, we estimate the electron-phonon limited electrical conductivity σ of Bi_2Se_3 in the in-plane direction as a function of temperature for different values of n-type doping concentrations (results for p-type doping are reported in the supplementary material). In the supplementary material, we briefly discuss a comparison with available experimental results which, for the purpose of the present study, show a good qualitative agreement. In the figure, dashed lines are the semiclassical estimates σ^{BTE}, while solid lines the estimates using the WTE. For the highest doping values, when the chemical potential shifts into the conduction band, the conductivity has the typical metallic-like behavior of decreasing with temperature. Under these conditions, BTE and WTE do not differ significantly, except at larger temperatures.

For smaller doping concentrations the chemical potential lies in the band gap and we thus observe a semiconducting behavior of σ increasing with temperature. The semiclassical model predicts a smaller conductivity than the WTE estimate. In fact, when only a few carriers from the bottom of the conduction band are excited, the average carriers' group velocity is small, due to the quadratic nature of the band minimum. Therefore, the semiclassical contribution to electrical conductivity tends to be rather small. The WTE corrects this picture, including the Zener tunneling effect [7]. As carriers from valence and conduction band are close in energy, they can interact and contribute to the electrical transport through the tunneling effect, as discussed above. For small dopings, the

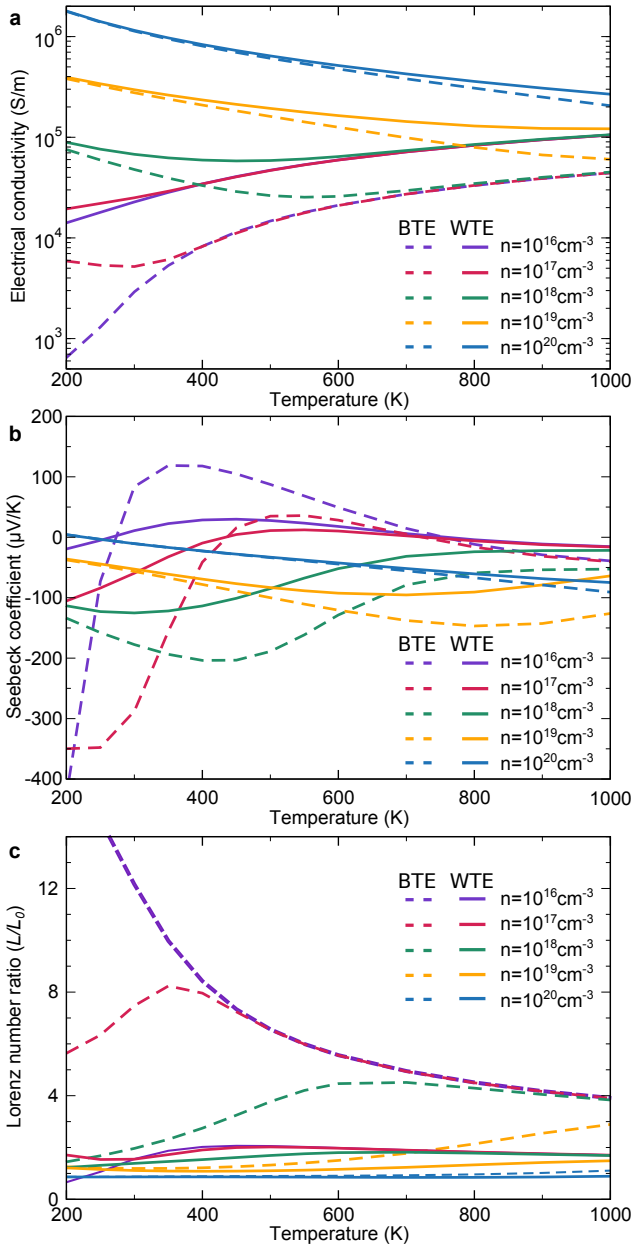

[h]

Figure 2: Computational estimates of the in-plane electrical conductivity (panel a), Seebeck coefficient (panel b), and Lorenz number ratio (panel c, see text for description) of Bi_2Se_3 as a function of temperature, for different values of electron doping concentration. Solid lines are estimated using the Wigner transport equation, while dotted lines are semiclassical estimates obtained solving the Boltzmann transport equation. For small doping concentrations, the interaction between electrons and holes significantly affect the estimates of transport coefficients.

WTE correction is significant, and can be much larger than the BTE conductivity value. For the smallest value of doping reported (10^{16}cm^{-3}), this correction is largest at lower temperatures. The doping of 10^{18}cm^{-3} is an intermediate case, with metallic behavior at low temperatures (and thus smaller WTE correction) and semiconducting (with larger WTE correction) at higher temperatures as the chemical potential moves from the band gap into the conduction band. We can thus conclude that a substantial portion of electrical current at low doping is carried through the Zener tunneling included in the WTE formalism: the current is not only caused by the carriers traveling at a finite group velocity, but also by carriers' tunneling between single-particle Bloch states.

In Fig. 2b. we report the Seebeck coefficient S, solid/dashed lines are WTE/BTE estimates. The negative values indicate that a majority of carriers are electrons, although, in a small band gap system, deviations from this behavior can occur. In a parabolic band model treated semiclassically, S is proportional to the logarithmic derivative of the density of states [34]. Therefore, at low temperatures, one expects the Seebeck coefficient to increase as the doping concentration is decreased. This phenomenon is crucial to optimize the thermoelectric efficiency, where the goal is to maximize the power factor σS^2. However, within the WTE, S is not anymore simply related to the density of states, as additional terms in the transport equations appear (as detailed in the supplementary information). As a result, the large increase of the Seebeck coefficient expected by a semiclassical model at low doping is strongly suppressed by the WTE, and S becomes comparable to its values at high doping. We thus conclude that the tunneling effects captured by the WTE can alter considerably the predictions of thermoelectric properties in narrow-gap semiconductors.

We now examine the relationship of electrical conductivity σ and open-circuit electronic thermal conductivity κ_{el}. The Wiedemann-Franz (WF) law defines the Lorenz number $L = \frac{\kappa_{\text{el}}}{\sigma T}$, which in the ideal metallic limit is a constant $L_0 = 2.44 \cdot 10^{-8}$ $\text{W}\Omega\text{K}^{-2}$. Knowledge of L is necessary to decouple the electronic contribution κ_{el} and the lattice contribution κ_{ph} from measurements of the total κ. In Fig. 2c, we plot the computed ratio $\frac{L}{L_0}$ for several doping concentrations and temperatures, using both BTE and WTE. At high doping the system has metallic character, and both predictions closely follow the WF law. In the case of small doping, in the bipolar regime, the semiclassical BTE predicts large deviations from the WF law, as has been discussed previously [13, 35, 36, 37]. Remarkably, in the WTE solution the Lorenz numbers are much closer to the expected range for semiconductors, indicating that quantum transport effects included in the WTE strongly suppress bipolar deviations and work towards restoring the validity of the WF law.

In Fig. 3a, we analyze the contributions to the BTE electrical conductivity as a function of the carriers' energy at doping concentration of 10^{18} cm^{-3}, and temperature of 700 K. This histogram is built such that the area under the curve integrates to the total electrical conductivity. Within the semiclassical relaxation time approximation, the quantity plotted is an energy-resolved histogram of $\frac{2e^2}{VN_k}\frac{\partial \bar{f}_b(\boldsymbol{k})}{\partial \epsilon} v_{bb}^2(\boldsymbol{k}) \frac{1}{\Gamma_b(\boldsymbol{k})}$, i.e. the contribution of a single mode to the BTE electrical conductivity. As expected, the dominant contributions to electrical conductivity come from carriers whose energy is close to the chemical potential (set at 0 eV). The contributions of other carriers decay exponentially as their energy gets further from the chemical potential.

The WTE correction $\Delta\sigma$ cannot be resolved in terms of a single carrier's energy, since it involves the tunneling between two states at different energies. Therefore, in Fig. 3b, we plot the contributions to the electrical conductivity as a function of two interacting carriers energies. On the diagonal, we find again the BTE-like terms shown in Fig. 3a. In addition, we can see important off-diagonal contributions to the electrical conductivity that are not present in the BTE and are introduced with the WTE. In particular, there are two peaks of contributions to electrical conductivity, that couple electrons of energy 1.0 eV with holes at -0.8 eV. These two values correspond to the average energies of the valence and conduction bands, when the DOS reaches the corresponding maximum values. Therefore, in contrast to the typical intuition of the Zener tunneling, we find that the most

significant coupling between carriers takes place far from the chemical potential, with carriers of energy much larger than the thermal energy. For this material, the dipole interaction between carriers in subvalleys of the valence and conduction is thus particularly strong, allowing for high-energy carriers to contribute to transport. As a result, we speculate that Zener tunneling may take place also in semiconductors with a wide gap and contribute significantly to electrical conductivity, provided that the inter-band dipole interaction is sufficiently strong, for instance in materials with high optical absorption character.

In conclusion, we have shown that the Moyal equation of motion for the Wigner function leads to a straightforward extension of the Boltzmann transport equation, which takes into account additional quantum transport effects such as Zener tunneling. With this new Wigner transport equation formalism it is possible to compute the full set of Onsager transport coefficients for thermal and electrical transport from first principles, starting with density functional perturbation theory. We implemented this equation and solved it for the topological insulator Bi_2Se_3. We have shown that, while at high doping concentrations the Boltzmann equation provides a fairly accurate description of transport, it fails at low doping concentrations. At low dopings, the Zener tunneling effect contributes significantly to the electronic transport, modifying both electrical conductivity and Seebeck coefficient. Lastly, we have shown that Zener tunneling does not just take place across the states closest to the band gap, but can involve states that are significantly further apart in energy, provided that the dipole interaction is sufficiently strong. As a result, we have extended the range of applicability of ab-initio transport simulations to materials where quantum tunneling effects couple carriers, and a semiclassical description is no longer adequate.

Supplementary material

0.1 Equation of motion of the Wigner function

In this section, we detail the derivation of the Wigner transport equation discussed in the main text.

We start from the single-particle Hamiltonian H of an electron in a crystal in presence of an electric field, that is

$$H = H_0 + e\boldsymbol{x} \cdot \boldsymbol{E} = H_0 + \boldsymbol{d} \cdot \boldsymbol{E} \,, \tag{8}$$

where H_0 is the Hamiltonian of a crystal in its ground state, e the electronic charge, $\boldsymbol{x}$ the position operator, $\boldsymbol{E}$ the electric field and $\boldsymbol{d} = e\boldsymbol{x}$ the dipole operator. We further make the hypothesis that the electric field can be added as a perturbation, so that the eigenvectors $|\psi_{\boldsymbol{k}b}\rangle$ of H are approximately the eigenvectors of H_0 as well (with Bloch quantum numbers $\boldsymbol{k}$ for the wavevector and b for the band index). The eigenvalues of H_0 are denoted as $\epsilon_b(\boldsymbol{k})$. We also stress that the single-particle approximation is consistent with the numerical implementation using parameters computed from density-functional theory.

Before proceeding, it is important to choose a wavefunction gauge such that the derivative $\frac{\partial|\psi_{\boldsymbol{k}b}\rangle}{\partial \boldsymbol{k}}$ exists and is continuous. To this aim, we recall that the maximally localized Wannier functions are written as

$$|\boldsymbol{R}n\rangle = \frac{V}{(2\pi)^3}\int d\boldsymbol{k} e^{-i\boldsymbol{k}\cdot\boldsymbol{R}} \sum_b U_{\boldsymbol{k},bn}\,|\psi_{\boldsymbol{k}b}\rangle = \frac{V}{(2\pi)^3}\int d\boldsymbol{k} e^{-i\boldsymbol{k}\cdot\boldsymbol{R}}\,|\tilde{\psi}_{\boldsymbol{k}n}\rangle \;, \tag{9}$$

where $\boldsymbol{R}$ labels a Bravais lattice site and $U_{\boldsymbol{k},mn}$ is a matrix fixing the wavefunction gauge. The matrix $U_{\boldsymbol{k},bn}$ is chosen as the one that maximally localizes Wannier functions [38], which has also the benefit of making $|\tilde{\psi}_{\boldsymbol{k}n}\rangle$ a smooth wavefunction across different wavevectors (otherwise, wavefunctions at different wavevectors assume random phases).

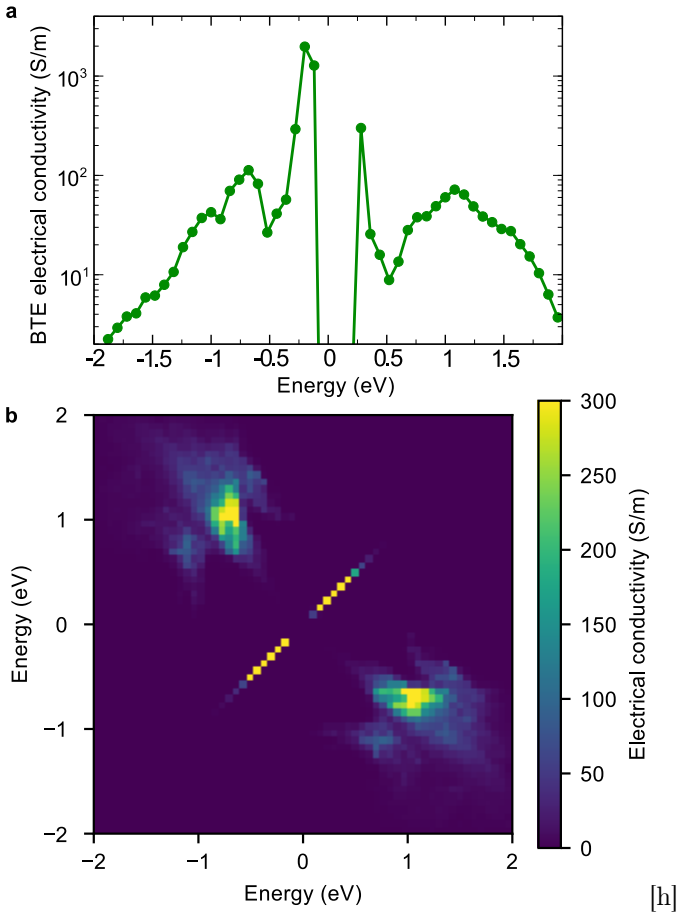

[h]

Figure 3: Panel a: histogram of contributions to semiclassical electrical conductivity as a function of the carrier energy, for Bi_2Se_3 at 700K and n-doping at 10^{18} cm^{-3}. Panel b, 2D histogram of contributions to the electrical conductivity for the same system as estimates with the Wigner transport equation against the energy of two coupled carriers. Off-diagonal contributions represent electrical conductivity arising from the coupling between electrons and holes.

Next, we briefly recall the definition of the Wigner transform. Given an operator in the real-space (position) representation $A(\boldsymbol{x}, \boldsymbol{x'})$, we can transform it to the phase-space representation through the Wigner transform $W[\cdot]$, defined as

$$W[A]_{nn'}(\boldsymbol{x}, \boldsymbol{k}) = \int d\boldsymbol{x'} e^{-i2\boldsymbol{k}\cdot\boldsymbol{x'}} A_{nn'}(\boldsymbol{x} + \boldsymbol{x'}, \boldsymbol{x} - \boldsymbol{x'}) \ . \tag{10}$$

Similarly, if we start from an operator in the momentum representation, we can transform it into the phase-space representation as

$$W[A]_{nn'}(\boldsymbol{x}, \boldsymbol{k}) = \int d\boldsymbol{k'} e^{i2\boldsymbol{k'}\cdot\boldsymbol{x}} A_{nn'}(\boldsymbol{k} + \boldsymbol{k'}, \boldsymbol{k} - \boldsymbol{k'}) \ . \tag{11}$$

We now want to describe the equation of motion of the system under the Hamiltonian of Eq. 8. We can build the density matrix of the system using the basis of wavefunctions in the Wannier gauge $|\tilde{\psi}_{\boldsymbol{k}n}\rangle$ introduced above. We thus represent the state of the system using the single-particle density matrix operator ρ, whose matrix elements are $\rho_{nn'}(\boldsymbol{k}, \boldsymbol{k'}; t) = \mathrm{Tr}\{\hat{\rho}(t) c^{\dagger}_{\boldsymbol{k'},n'} c_{\boldsymbol{k},n}\}$, where $c^{\dagger}_{\boldsymbol{k},n}$, and $c_{\boldsymbol{k},n}$ are creation/annihilation operators of an electronic state $|\tilde{\psi}_{\boldsymbol{k}n}\rangle$. As described in Ref. [18], one may use the equation of motion of the density matrix, and Wigner transform it to derive an equation of motion for the system. Here, we derive a simplified equation of motion for the state of the system using the Wigner function of the crystal [15], which is defined through the Wigner transform of the density matrix as

$$W_{nn'}(\boldsymbol{x}, \boldsymbol{k}, t) = \sum_{\Delta\boldsymbol{k}} e^{i2\Delta\boldsymbol{k}\cdot\boldsymbol{x}} \rho_{nn'}\Big(\boldsymbol{k} + \Delta\boldsymbol{k}, \boldsymbol{k} - \Delta\boldsymbol{k}; t\Big) \ , \tag{12}$$

where we used the rotation of coordinates $\boldsymbol{k}, \boldsymbol{k'} \to \frac{\boldsymbol{k}+\boldsymbol{k'}}{2}, \Delta\boldsymbol{k} = \boldsymbol{k'} - \boldsymbol{k}$.

Note that that the position $\boldsymbol{x}$ appearing in the Wigner transform is, to be precise, a Bravais lattice vector and thus a discrete variable. However, when studying transport properties, we are only interested in the macroscopic behavior of the system. Under this macroscopic limit, we only study the changes of $\boldsymbol{x}$ on a length-scale much larger than the lattice parameter, so that $\boldsymbol{x}$ can be approximated as a continuum variable. As a result, W admits a continuous derivative with respect to $\boldsymbol{x}$ and, thanks to the gauge choice on the wavefunction, W is also differentiable with respect to $\boldsymbol{k}$.

As demonstrated by Moyal [16, 17], the Wigner function obeys the following equation of motion:

$$\frac{\partial W_{nn'}(\boldsymbol{x}, \boldsymbol{k}, t)}{\partial t} = -\big\{\big\{W(\boldsymbol{x}, \boldsymbol{k}, t), H(\boldsymbol{x}, \boldsymbol{k})\big\}\big\}_{nn'} = \frac{i}{\hbar}\big(W(\boldsymbol{x}, \boldsymbol{k}, t) \star H(\boldsymbol{x}, \boldsymbol{k}) - H(\boldsymbol{x}, \boldsymbol{k}) \star W(\boldsymbol{x}, \boldsymbol{k}, t)\big)_{nn'} \ , \tag{13}$$

where $\{\{f, g\}\}$ indicates the Moyal bracket between two operators f and g, and the Moyal product $\star$ is defined as:

$$f \star g = f(\boldsymbol{x}, \boldsymbol{k}) \exp\left(\frac{i}{2}\left(\frac{\overleftarrow{\partial}}{\partial \boldsymbol{x}} \cdot \frac{\vec{\partial}}{\partial \boldsymbol{k}} - \frac{\overleftarrow{\partial}}{\partial \boldsymbol{k}} \cdot \frac{\vec{\partial}}{\partial \boldsymbol{x}}\right)\right) g(\boldsymbol{x}, \boldsymbol{k}) \ , \tag{14}$$

where the left/right arrow indicates that the derivative operator acts on the operator to the left/right.

The equation of motion for W is the phase-space analogous of the Liouville-Von Neumann equation of motion for the density matrix, and therefore has a complexity comparable to that of Schroedinger's equation.

Now, we can further simplify this equation of motion by making the hypothesis that both H and W are slowly varying functions of $\boldsymbol{x}$ and $\boldsymbol{k}$. We then expand the exponential appearing in the Moyal

product in Taylor series and approximate the equation of motion as

$$\frac{\partial W_{nn'}(\boldsymbol{x},\boldsymbol{k},t)}{\partial t} \approx i\Big(W(\boldsymbol{x},\boldsymbol{k},t)H(\boldsymbol{x},\boldsymbol{k}) - H(\boldsymbol{x},\boldsymbol{k})W(\boldsymbol{x},\boldsymbol{k},t)\Big)_{nn'} - \frac{1}{2}\bigg(W(\boldsymbol{x},\boldsymbol{k},t)\Big(\frac{\overleftarrow{\partial}}{\partial \boldsymbol{x}}\cdot\frac{\vec{\partial}}{\partial \boldsymbol{k}} - \frac{\overleftarrow{\partial}}{\partial \boldsymbol{k}}\cdot\frac{\vec{\partial}}{\partial \boldsymbol{x}}\Big)H(\boldsymbol{x},\boldsymbol{k}) - H(\boldsymbol{x},\boldsymbol{k})\Big(\frac{\overleftarrow{\partial}}{\partial \boldsymbol{x}}\cdot\frac{\vec{\partial}}{\partial \boldsymbol{k}} - \frac{\overleftarrow{\partial}}{\partial \boldsymbol{k}}\cdot\frac{\vec{\partial}}{\partial \boldsymbol{x}}\Big)W(\boldsymbol{x},\boldsymbol{k},t)\bigg)_{nn'} \tag{15}$$

$$= -i\Big[H(\boldsymbol{x},\boldsymbol{k}),W(\boldsymbol{x},\boldsymbol{k},t)\Big]_{nn'} - \frac{1}{2}\Big\{\frac{\partial H(\boldsymbol{x},\boldsymbol{k})}{\partial \boldsymbol{k}},\cdot\frac{\partial W(\boldsymbol{x},\boldsymbol{k},t)}{\partial \boldsymbol{x}}\Big\}_{nn'} + \frac{1}{2}\Big\{\frac{\partial H(\boldsymbol{x},\boldsymbol{k})}{\partial \boldsymbol{x}},\cdot\frac{\partial W(\boldsymbol{x},\boldsymbol{k},t)}{\partial \boldsymbol{k}}\Big\}_{nn'} . \tag{16}$$

Note that, if H and W commute (for example, if the two are diagonal in the band index n), this equation reduces to the Poisson bracket, i.e. the time evolution of a classical Hamiltonian.

The equation of motion is almost in the final form reported in the main text. However, it is still expressed in terms of the basis set $|\tilde{\psi}_{\boldsymbol{k}n}\rangle$. While convenient for the derivation, it is more practical to work with an equation in terms of the Bloch index b, rather than the Wannier index n (the Wannier function basis set doesn't in general diagonalize the Bloch Hamiltonian). Therefore, we rotate results in the $|\psi_{\boldsymbol{k}b}\rangle$ basis set and write W and H as:

$$H_{bb'}(\boldsymbol{x},\boldsymbol{k}) = \sum_{nn'} U^{\dagger}_{bn}(\boldsymbol{k})H_{nn'}(\boldsymbol{x},\boldsymbol{k})U_{b'n'}(\boldsymbol{k}) , \tag{17}$$

and

$$f_{bb'}(\boldsymbol{x},\boldsymbol{k}) = \sum_{nn'} U^{\dagger}_{bn}(\boldsymbol{k})W_{nn'}(\boldsymbol{x},\boldsymbol{k})U_{b'n'}(\boldsymbol{k}) . \tag{18}$$

The equation of motion can thus be written as:

$$\frac{\partial f_{bb'}(\boldsymbol{x},\boldsymbol{k},t)}{\partial t} = -i\Big[H(\boldsymbol{x},\boldsymbol{k}),f(\boldsymbol{x},\boldsymbol{k},t)\Big]_{bb'} - \frac{1}{2}\Big\{\frac{\partial H(\boldsymbol{x},\boldsymbol{k})}{\partial \boldsymbol{k}},\cdot\frac{\partial f(\boldsymbol{x},\boldsymbol{k},t)}{\partial \boldsymbol{x}}\Big\}_{bb'} + \frac{1}{2}\Big\{\frac{\partial H(\boldsymbol{x},\boldsymbol{k})}{\partial \boldsymbol{x}},\cdot\frac{\partial f(\boldsymbol{x},\boldsymbol{k},t)}{\partial \boldsymbol{k}}\Big\}_{bb'} . \tag{19}$$

We now want to manipulate the matrix elements of the Hamiltonian entering the equation of motion for the Wigner function. First, we note that the Wigner transform of the Hamiltonian at Eq. 8 is Eq. 8 itself, because H_0 (a Bloch Hamiltonian) is diagonal in $\boldsymbol{k}$ and the coupling with the electric-field is diagonal in $\boldsymbol{x}$. The matrix elements of such Hamiltonian are

$$\langle\psi_{\boldsymbol{k}b}\,|\,H(\boldsymbol{x},\boldsymbol{k})\,|\,\psi_{\boldsymbol{k}b'}\rangle = \epsilon_b(\boldsymbol{k})\delta_{bb'} + \boldsymbol{d}_{bb'}(\boldsymbol{k})\cdot\boldsymbol{E} = [\mathcal{E}(\boldsymbol{k}) + \boldsymbol{D}(\boldsymbol{k})\cdot\boldsymbol{E}]_{bb'} , \tag{20}$$

where we introduced two matrices $\mathcal{E}(\boldsymbol{k})$ and $\boldsymbol{D}(\boldsymbol{k})$ containing the single-particle energies $\epsilon_b(\boldsymbol{k})$ and dipoles $\boldsymbol{d}_{bb'}(\boldsymbol{k})$. The dipole operator requires some care, since the position operator is not well-defined in a periodic system. The off-diagonal terms $b \neq b'$ satisfy:

$$\boldsymbol{d}_{\boldsymbol{k},bb'} = \langle\psi_{\boldsymbol{k}b}\,|\,e\boldsymbol{r}\,|\,\psi_{\boldsymbol{k}b'}\rangle = e\frac{\langle\psi_{\boldsymbol{k}b}\,|\,[H^0,\boldsymbol{r}]\,|\,\psi_{\boldsymbol{k}b'}\rangle}{\epsilon_b(\boldsymbol{k}) - \epsilon_{b'}(\boldsymbol{k})} = -ie\frac{\boldsymbol{v}_{bb'}(\boldsymbol{k})}{\epsilon_b(\boldsymbol{k}) - \epsilon_{b'}(\boldsymbol{k})}, \quad \text{for } b \neq b' , \tag{21}$$

where $\boldsymbol{v}_{bb'}(\boldsymbol{k})$ is the velocity operator. The diagonal terms $d_{bb}(\boldsymbol{k})$ are ill-defined [39]. Luckily, these terms appear only inside a commutator, so that the diagonal terms don't contribute. We thus set $d_{bb}(\boldsymbol{k}) = 0$ without altering results.

The derivatives of the Hamiltonian are readily computed as

$$\left\langle\psi_{\boldsymbol{k}b}\right|\frac{\partial H(\boldsymbol{x},\boldsymbol{k})}{\partial \boldsymbol{x}}\left|\psi_{\boldsymbol{k}b'}\right\rangle = e\boldsymbol{E}\delta_{bb'} , \tag{22}$$

and

$$\left\langle \psi_{\boldsymbol{k}b} \middle| \frac{\partial H(\boldsymbol{x},\boldsymbol{k})}{\partial \boldsymbol{k}} \middle| \psi_{\boldsymbol{k}b'} \right\rangle = v_{bb'}(\boldsymbol{k}) \; . \tag{23}$$

Combining all this terms together, the equation of motion for the Wigner function $f_{bb'}(\boldsymbol{x},\boldsymbol{k},t)$ is

$$\frac{\partial f_{bb'}(\boldsymbol{x},\boldsymbol{k},t)}{\partial t} + i\Big[\mathcal{E}(\boldsymbol{k}) + \boldsymbol{D}(\boldsymbol{k})\cdot\boldsymbol{E}, f(\boldsymbol{x},\boldsymbol{k},t)\Big]_{bb'} + \frac{1}{2}\Big\{\boldsymbol{v}(\boldsymbol{k}), \cdot\frac{\partial f(\boldsymbol{x},\boldsymbol{k},t)}{\partial \boldsymbol{x}}\Big\}_{bb'} - e\boldsymbol{E}\cdot\frac{\partial f_{bb'}(\boldsymbol{x},\boldsymbol{k},t)}{\partial \boldsymbol{k}} = 0 \; . \tag{24}$$

This is the equation of motion for the Hamiltonian $H_0 + e\boldsymbol{x}\cdot\boldsymbol{E}$, which, however, doesn't take into account for the effect of electronic collisions, in particular electron-phonon scattering. This effect is added as a perturbation, and we define the electron-phonon collision matrix as [18, 19, 20, 21, 22]:

$$\left.\frac{\partial f_{bb'}(\boldsymbol{x},\boldsymbol{k},t)}{\partial t}\right|_{coll} = (1-\delta_{bb'})\frac{\Gamma_b(\boldsymbol{k})+\Gamma_{b'}(\boldsymbol{k})}{2} f_{bb'}(\boldsymbol{x},\boldsymbol{k},t) + \delta_{bb'}\frac{1}{V}\sum_{\boldsymbol{k}'b'} A_{\boldsymbol{k}b,\boldsymbol{k}'b'} f_{b'b'}(\boldsymbol{x},\boldsymbol{k}',t) \; . \tag{25}$$

Here, the diagonal terms of f are modified by the scattering matrix A, which is built as the electron-phonon collision matrix of the Boltzmann transport equation. The off-diagonal terms instead are built [40, 18, 41], from the electron-phonon linewidths $\Gamma_b(\boldsymbol{k}) = A_{\boldsymbol{k}b,\boldsymbol{k}b}$. The electron-phonon scattering matrix is computed as [34]:

$$\begin{aligned}
A_{\boldsymbol{k}b,\boldsymbol{k}'b'} =& \delta_{\boldsymbol{k}\boldsymbol{k}'}\delta_{bb'}\frac{2\pi}{N_{\boldsymbol{q}}}\sum_{m\nu\boldsymbol{q}} |g_{mn\nu}(\boldsymbol{k},\boldsymbol{q})|^2 \Big[\big(1-\bar{f}_m(\boldsymbol{k}+\boldsymbol{q})+\bar{n}_\nu(\boldsymbol{q})\big)\delta\big(\epsilon_n(\boldsymbol{k})-\epsilon_m(\boldsymbol{k}+\boldsymbol{q})-\omega_\nu(\boldsymbol{q})\big) \\
&+ \big(\bar{f}_m(\boldsymbol{k}+\boldsymbol{q})+\bar{n}_\nu(\boldsymbol{q})\big)\delta\big(\epsilon_n(\boldsymbol{k})-\epsilon_m(\boldsymbol{k}+\boldsymbol{q})+\omega_\nu(\boldsymbol{q})\big)\Big] \\
&+ \frac{2\pi}{N_{\boldsymbol{q}}}\sum_{m\nu\boldsymbol{q}} |g_{mn\nu}(\boldsymbol{k},\boldsymbol{q})|^2 \Big[\bar{f}_n(\boldsymbol{k})\big(1-\bar{f}_m(\boldsymbol{k}+\boldsymbol{q})\big)\bar{n}_\nu(\boldsymbol{q})\delta\big(\epsilon_n(\boldsymbol{k})-\epsilon_m(\boldsymbol{k}+\boldsymbol{q})+\omega_\nu(\boldsymbol{q})\big) \\
&+ \bar{f}_m(\boldsymbol{k}+\boldsymbol{q})\big(1-\bar{f}_n(\boldsymbol{k})\big)\bar{n}_\nu(\boldsymbol{q})\delta\big(\epsilon_n(\boldsymbol{k})-\epsilon_m(\boldsymbol{k}+\boldsymbol{q})-\omega_\nu(\boldsymbol{q})\big)\Big] \; ,
\end{aligned} \tag{26}$$

where $\omega_\nu(\boldsymbol{q})$ is the phonon frequency at wavevector $\boldsymbol{q}$ and branch index ν, $\bar{n}_\nu(\boldsymbol{q})$ is the Bose–Einstein distribution function, and $|g_{mn\nu}(\boldsymbol{k},\boldsymbol{q})|^2$ is the strength of the electron-phonon interaction. All these quantities can be computed using density-functional perturbation theory.

Finally, the WTE becomes

$$\frac{\partial f_{bb'}(\boldsymbol{x},\boldsymbol{k},t)}{\partial t} + i\Big[\mathcal{E}(\boldsymbol{k}) + \boldsymbol{D}(\boldsymbol{k})\cdot\boldsymbol{E}, f(\boldsymbol{x},\boldsymbol{k},t)\Big]_{bb'} + \frac{1}{2}\Big\{\boldsymbol{v}(\boldsymbol{k}), \cdot\frac{\partial f(\boldsymbol{x},\boldsymbol{k},t)}{\partial \boldsymbol{x}}\Big\}_{bb'} - e\boldsymbol{E}\cdot\frac{\partial f_{bb'}(\boldsymbol{x},\boldsymbol{k},t)}{\partial \boldsymbol{k}} = -\left.\frac{\partial f_{bb'}(\boldsymbol{x},\boldsymbol{k},t)}{\partial t}\right|_{coll} \; . \tag{27}$$

0.2 Solution of the Wigner transport equation and transport properties

In this section, we show how to solve the Wigner transport equation for a bulk system at the steady-state.

First, we study the response of the system to an electric field. In this case the Wigner function simplifies considerably, since it doesn't depend on time or space, and we can thus simply indicate it as $f_{bb'}(\boldsymbol{k})$. Once computed $f_{bb'}(\boldsymbol{k})$, we will show in the next section how to evaluate transport coefficients.

For small deviations from equilibrium, we linearize the Wigner distribution function as

$$f_{bb'}(\boldsymbol{k}) = \bar{f}_b(\boldsymbol{k})\delta_{bb'} + f^E_{bb'}(\boldsymbol{k})\cdot\boldsymbol{E} \; , \tag{28}$$

where $\bar{f}$ is the Fermi–Dirac distribution, and f^E is the unknown quantity to be found from the WTE. Note that f^E is a vector to be found for every direction in which the electric field is applied.

We split the solution of the WTE in two parts, diagonal ($b = b'$) and off-diagonal ($b \neq b'$) contributions. The diagonal components of the WTE are

$$e\boldsymbol{E} \cdot \frac{\partial f_{bb}(\boldsymbol{k})}{\partial \boldsymbol{k}} = \sum_{\boldsymbol{k}'b'} A_{\boldsymbol{k}b,\boldsymbol{k}'b'} f_{b'b'}(\boldsymbol{k}') \;, \tag{29}$$

which is equivalent to the BTE problem. The equation can thus be solved using standard techniques developed for the BTE (see e.g. Ref. [42]). We verified that exact solutions of the BTE don't modify results significantly, and therefore we adopt the relaxation time approximation, and approximate the diagonal WTE as

$$e\boldsymbol{E} \cdot \frac{\partial f_{bb}(\boldsymbol{k})}{\partial \boldsymbol{k}} = \Gamma_b(\boldsymbol{k}) f_{bb}(\boldsymbol{k}) \;. \tag{30}$$

Using the linearized expression for the Wigner function (and neglecting terms quadratic in $\boldsymbol{E}$), the equation is readily solved by

$$f^E_{bb}(\boldsymbol{k}) = \frac{e}{\Gamma_b(\boldsymbol{k})} \frac{\partial \bar{f}_b(\boldsymbol{k})}{\partial \boldsymbol{k}} \;. \tag{31}$$

The off-diagonal terms evolve according to

$$\frac{i}{\hbar}\Big[\mathcal{E}(\boldsymbol{k}) + \boldsymbol{D}(\boldsymbol{k}) \cdot \boldsymbol{E}, f(\boldsymbol{k})\Big]_{bb'} - e\boldsymbol{E} \cdot \frac{\partial f_{bb'}(\boldsymbol{k})}{\partial \boldsymbol{k}} = -\frac{\Gamma_b(\boldsymbol{k}) + \Gamma_{b'}(\boldsymbol{k})}{2} f_{bb'}(\boldsymbol{k}) \;. \tag{32}$$

Using the linearized expression, we obtain:

$$i\Big(\epsilon_b(\boldsymbol{k}) - \epsilon_{b'}(\boldsymbol{k})\Big) f^E_{bb'}(\boldsymbol{k}) + i\Big(\bar{f}_{b'}(\boldsymbol{k}) - \bar{f}_b(\boldsymbol{k})\Big) \boldsymbol{d}_{bb'}(\boldsymbol{k}) = -\frac{\Gamma_b(\boldsymbol{k}) + \Gamma_{b'}(\boldsymbol{k})}{2} f^E_{bb'}(\boldsymbol{k}) \;. \tag{33}$$

The equation is readily solved finding

$$f^E_{bb'}(\boldsymbol{k}) = \frac{\bar{f}_b(\boldsymbol{k}) - \bar{f}_{b'}(\boldsymbol{k})}{\epsilon_b(\boldsymbol{k}) - \epsilon_{b'}(\boldsymbol{k})} \frac{2e\boldsymbol{v}_{bb'}(\boldsymbol{k})}{2i\big(\epsilon_b(\boldsymbol{k}) - \epsilon_{b'}(\boldsymbol{k})\big) + \big(\Gamma_b(\boldsymbol{k}) + \Gamma_{b'}(\boldsymbol{k})\big)} \;. \tag{34}$$

Similarly, we can solve the WTE for the response to a thermal gradient, similarly to what discussed in Ref. [18]. We can now set the electric field to zero and linearize the Wigner function as:

$$f_{bb'}(\boldsymbol{k}) = \bar{f}_b(\boldsymbol{k})\delta_{bb'} + f^T_{bb'}(\boldsymbol{k}) \cdot \boldsymbol{\nabla} T \;. \tag{35}$$

The diagonal components of the WTE are then

$$\boldsymbol{v}(\boldsymbol{k}) \frac{\partial \bar{f}_b(\boldsymbol{k})}{\partial T} = -\sum_{\boldsymbol{k}'b'} A_{\boldsymbol{k}b,\boldsymbol{k}'b'} f^T_{b'b'}(\boldsymbol{k}') \;, \tag{36}$$

which can be solved in the relaxation time approximation as discussed above for the electrical conductivity. The off-diagonal components are given by

$$i\Big(\epsilon_b(\boldsymbol{k}) - \epsilon_{b'}(\boldsymbol{k})\Big) f^T_{bb'}(\boldsymbol{k}) + \frac{1}{2}\left(\frac{\partial \bar{f}_{b'}(\boldsymbol{k})}{\partial T} + \frac{\partial \bar{f}_b(\boldsymbol{k})}{\partial T}\right) \boldsymbol{v}_{bb'}(\boldsymbol{k}) = -\frac{\Gamma_b(\boldsymbol{k}) + \Gamma_{b'}(\boldsymbol{k})}{2} f^T_{bb'}(\boldsymbol{k}) \;, \tag{37}$$

which can again be solved trivially in terms of $f^T_{bb'}(\boldsymbol{k})$.

0.3 Transport coefficients

Having computed the Wigner function from the WTE, the expectation value of an operator A can be computed in the phase-space representation as

$$\langle A(t)\rangle = \frac{g_s}{VN_k}\sum_{\boldsymbol{k}bb'}\int f_{bb'}(\boldsymbol{x},\boldsymbol{k},t)A_{b'b}(\boldsymbol{k})d\boldsymbol{x}\ , \tag{38}$$

where the factor $g_s = 2$ takes into account for the spin-degeneracy (we are only considering non-magnetic systems), V is the volume of the crystal unit cell and N_k is a normalization for the number of wavevectors. We can apply this formula to estimate the current of a steady-state homogeneous system, i.e. when $f_{bb'}(\boldsymbol{x},\boldsymbol{k},t)$ doesn't depend on space and time. The charge current density $\boldsymbol{J}$ can be computed as:

$$\boldsymbol{J} = \frac{eg_s}{VN_k}\sum_{\boldsymbol{k}bb'} f_{bb'}(\boldsymbol{k})\boldsymbol{v}_{b'b}(\boldsymbol{k}) = \frac{eg_s}{2VN_k}\sum_{\boldsymbol{k}b}\Big\{\boldsymbol{v}(\boldsymbol{k}), f(\boldsymbol{k})\Big\}_{bb'}\ , \tag{39}$$

where we used an anticommutator to symmetrize results. The electrical conductivity easily follows, since $\boldsymbol{J} = \sigma\boldsymbol{E}$.

More precisely, we can define the Onsager transport coefficients as:

$$\boldsymbol{J} = L_{EE}\boldsymbol{E} + L_{ET}\nabla T\ , \tag{40}$$

$$\boldsymbol{Q} = L_{TE}\boldsymbol{E} + L_{TT}\nabla T\ , \tag{41}$$

where $\boldsymbol{Q}$ is the heat flux, and the response coefficients can be computed as:

$$L^{ij}_{EE} = \frac{eg_s}{VN_k}\sum_{\boldsymbol{k}b}\frac{1}{2}\Big\{v^i(\boldsymbol{k}), f^{E_j}(\boldsymbol{k})\Big\}_{bb}\ , \tag{42}$$

$$L^{ij}_{ET} = \frac{eg_s}{VN_k}\sum_{\boldsymbol{k}b}\frac{1}{2}\Big\{v^i(\boldsymbol{k}), f^{T_j}(\boldsymbol{k})\Big\}_{bb}\ , \tag{43}$$

$$L^{ij}_{TE} = \frac{g_s}{VN_k}\sum_{\boldsymbol{k}b}\big(\epsilon_b(\boldsymbol{k})-\mu\big)\frac{1}{2}\Big\{v^i(\boldsymbol{k}), f^{E_j}(\boldsymbol{k})\Big\}_{bb}\ , \tag{44}$$

$$L^{ij}_{TT} = \frac{g_s}{VN_k}\sum_{\boldsymbol{k}b}\big(\epsilon_b(\boldsymbol{k})-\mu\big)\frac{1}{2}\Big\{v^i(\boldsymbol{k}), f^{T_j}(\boldsymbol{k})\Big\}_{bb}\ . \tag{45}$$

As customary in transport theory [34], we recognize the electrical conductivity as $\sigma = L_{EE}$, the Seebeck coefficient as $S = -L^{-1}_{EE}L_{ET}$ and the thermal conductivity as $k = L_{TT} - L_{TE}L^{-1}_{EE}L_{ET}$.

The expression for the electrical conductivity is readily computed. In fact, we can write the electrical conductivity as

$$\sigma^{ij} = \sigma^{BTE,ij} + \Delta\sigma^{ij}\ , \tag{46}$$

where the first term takes into account for the diagonal (BTE-like) components of the WTE and the second one for the off-diagonal ones. Substituting the solution of the WTE in the definition of electrical conductivity, we find that the off-diagonal contribution is

$$\Delta\sigma^{ij} = \frac{eg_s}{2VN_k}\sum_{\boldsymbol{k}bb',b\neq b'}\big(v^i_{bb'}(\boldsymbol{k})f^{E_j}_{b'b}(\boldsymbol{k}) + f^{E_j}_{bb'}(\boldsymbol{k})v^i_{b'b}(\boldsymbol{k})\big) \tag{47}$$

$$= \frac{2g_se^2}{VN_k}\sum_{\boldsymbol{k}bb',b\neq b'} v^i_{bb'}(\boldsymbol{k})v^{j,*}_{b'b}(\boldsymbol{k})\frac{\bar{f}_{b'}(\boldsymbol{k})-\bar{f}_b(\boldsymbol{k})}{\epsilon_{b'}(\boldsymbol{k})-\epsilon_b(\boldsymbol{k})}\frac{\Gamma_b(\boldsymbol{k})+\Gamma_{b'}(\boldsymbol{k})}{4\big(\epsilon_{b'}(\boldsymbol{k})-\epsilon_b(\boldsymbol{k})\big)^2+(\Gamma_b(\boldsymbol{k})+\Gamma_{b'}(\boldsymbol{k}))^2}\ . \tag{48}$$

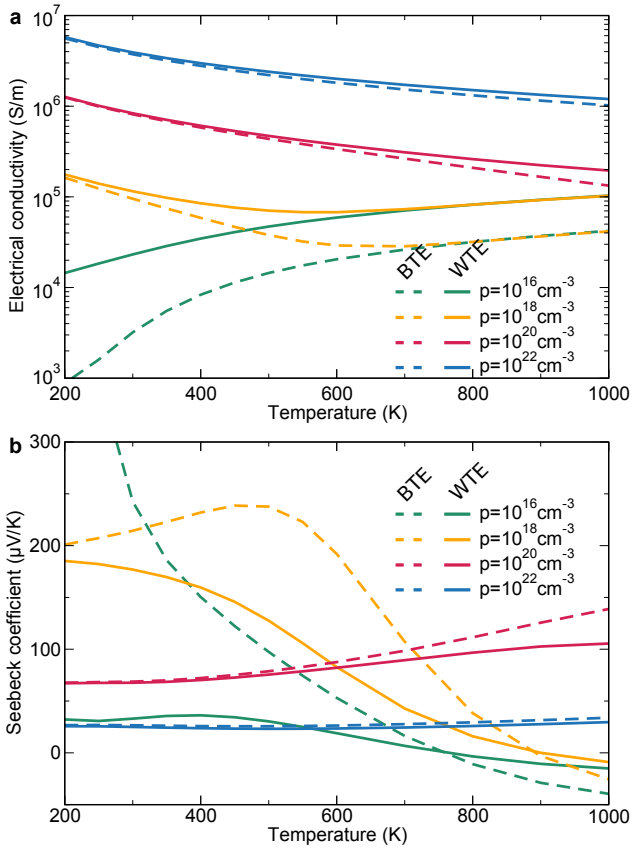

Figure 4: Computational estimates of the electrical conductivity (panel a) and Seebeck coefficient (panel b) of Bi_2Se_3 as a function of temperature, for different values of hole doping concentration. Solid lines are estimated using the Wigner transport equation, while dotted lines are semiclassical estimates obtained solving the Boltzmann transport equation. The hole doping case is qualitatively symmetric to the electron doping one discussed in the main text.

Note that $\Delta\sigma^{ij}$ is a positive quantity and therefore always increases the estimate of conductivity with respect to the BTE (since $\Gamma_{\boldsymbol{k},b} > 0$ and $\bar{f}$ is a decreasing monotonic function of ϵ) The diagonal contribution to the electrical conductivity is readily computed within the relaxation time approximation, and it can be shown to be

$$\sigma^{BTE,ij} = \frac{g_s}{VN_k}\sum_{\boldsymbol{k}b} e v^i_{bb}(\boldsymbol{k}) f^{E_j}_{bb}(\boldsymbol{k}) \approx \frac{g_s e^2}{VN_k}\sum_{\boldsymbol{k}b}\frac{\partial \bar{f}_b(\boldsymbol{k})}{\partial\epsilon} v^i_{bb}(\boldsymbol{k}) v^j_{bb}(\boldsymbol{k})\frac{1}{\Gamma_b(\boldsymbol{k})}\ . \tag{49}$$

0.4 Supplementary transport properties of Bi_2Se_3

In Fig. 4, we plot electrical conductivity and Seebeck coefficient for positive doping concentrations. Qualitatively, the data behave symmetrically to what discussed in the main text in the case of negatively-charged carriers concentrations.

In Fig. 5 we compare our model to available experimental data for bulk electrical conductivity.

At high doping concentrations, our results accurately reproduce the experimental measurement. At lower doping concentrations, the discrepancy between our simulations and experimental results increases, although qualitative trends appear still reproduced. It must be noted that there are several factors that might introduce discrepancies between experimental and simulation results. To mention some, the dependence of doping concentration on temperature is unclear and requires effort both in terms of modeling, as well as detailed temperature-dependent measurements of the Hall effect. Our simulations ignore electron-defect scattering, which may play a role especially at low temperatures. Finally, both experimental and theoretical values are affected by errors which may be hard to quantify (e.g. the dependence of computational results on the exchange-correlation functional chosen for the density functional theory calculation). Nevertheless, we emphasize that the qualitative trends discussed in the main text are robust and are not significantly altered by these considerations.

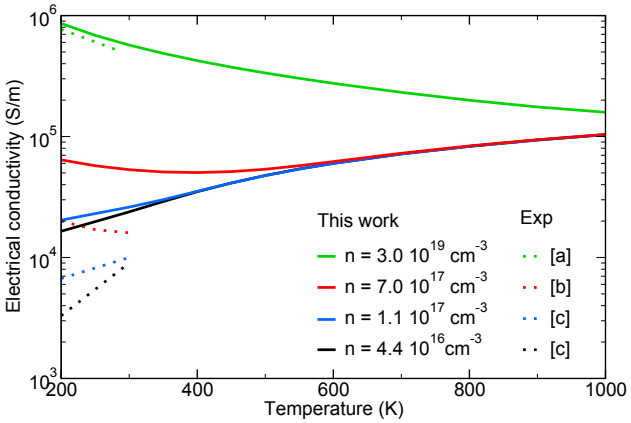

Figure 5: Computational estimates of the in-plane electrical conductivity of Bi_2Se_3 as a function of temperature, for different values of electron doping concentration using the Wigner transport equation (solid lines). We contrast these results against the experimental in-plane conductivity of single-crystals at negative doping concentrations of $3 \times 10^{19}\text{cm}^{-3}$ [43] (a), $7 \times 10^{17}\text{cm}^{-3}$ [44] (b), $4.4 \times 10^{16}\text{cm}^{-3}$ and $1.1 \times 10^{17}\text{cm}^{-3}$ [45] (c).

0.5 Methods

We use density functional theory as implemented in the plane-wave software suite Quantum-ESPRESSO [27, 28]. To compute the ground state, we use ultrasoft pseudopotentials from the GBRV library [46], with the PBEsol functional. We use an energy cutoff of 80 Ry, and integrate the Brillouin zone with a $8 \times 8 \times 8$ mesh of k-points. We build the trigonal unit cell using experimental estimates of the crystal structure [47], i.e. with a lattice parameter of 9.839 Å, and an angle α such that $\cos\alpha = 0.91068$. The Wannier functions are computed using p orbitals on both Bi and Se atoms as initial guesses.

Phonon properties, and the electron-phonon matrix elements are computed with density-functional perturbation theory [29] on a coarse grid of $4 \times 4 \times 4$ q-points. Electron-phonon matrix elements are subsequently interpolated on a finer grid of $39 \times 39 \times 39$ Brillouin zone wavevectors using a mixed Wannier and linear interpolation [12], while electronic energies and velocities are interpolated using Wannier90 [30]. Transport properties have been implemented in a custom-made software. The Dirac-delta ensuring energy conservation during an electron-phonon scattering event has been

approximated using an adaptive-smearing scheme [48]. Transport properties have been converged with respect to the k-points mesh used to integrate the Brillouin zone.

References

[1] Binghai Yan and Shou-Cheng Zhang. Topological materials. *Reports on Progress in Physics*, 75(9):096501, 2012.

[2] N. P. Armitage, E. J. Mele, and Ashvin Vishwanath. Weyl and dirac semimetals in three-dimensional solids. *Rev. Mod. Phys.*, 90:015001, Jan 2018.

[3] Lukas Müchler, Frederick Casper, Binghai Yan, Stanislav Chadov, and Claudia Felser. Topological insulators and thermoelectric materials. *Phys. Status Solidi RRL*, 7(1âĂŘ2):91–100, 2013.

[4] Joseph P. Heremans, Robert J. Cava, and Nitin Samarth. Tetradymites as thermoelectrics and topological insulators. *Nat. Rev. Mater.*, 2:17049, 2017.

[5] Pengzi Liu, James R. Williams, and Judy J. Cha. Topological nanomaterials. *Nat. Rev. Mater.*, 4:2058–8437, 2019.

[6] Niels Vandecasteele, Amelia Barreiro, Michele Lazzeri, Adrian Bachtold, and Francesco Mauri. Current-voltage characteristics of graphene devices: Interplay between zener-klein tunneling and defects. *Phys. Rev. B*, 82:045416, Jul 2010.

[7] Clarence Zener. A theory of the electrical breakdown of solid dielectrics. *Proc. R. Soc. Lond. A*, 145:523, 1934.

[8] Zhao Wang, Shidong Wang, Sergey Obukhov, Nathalie Vast, Jelena Sjakste, Valery Tyuterev, and Natalio Mingo. Thermoelectric transport properties of silicon: Toward an ab initio approach. *Phys. Rev. B*, 83:205208, May 2011.

[9] Wu Li. Electrical transport limited by electron-phonon coupling from boltzmann transport equation: An ab initio study of si, al, and mos_2. *Phys. Rev. B*, 92:075405, Aug 2015.

[10] S. Poncé, E.R. Margine, C. Verdi, and F. Giustino. Epw: Electron-phonon coupling, transport and superconducting properties using maximally localized wannier functions. *Comput. Phys. Comm.*, 209:116–133, 2016.

[11] Samuel Poncé, Elena R. Margine, and Feliciano Giustino. Towards predictive many-body calculations of phonon-limited carrier mobilities in semiconductors. *Phys. Rev. B*, 97:121201, Mar 2018.

[12] Mattia Fiorentini and Nicola Bonini. Thermoelectric coefficients of n-doped silicon from first principles via the solution of the boltzmann transport equation. *Phys. Rev. B*, 94:085204, Aug 2016.

[13] Georgy Samsonidze and Boris Kozinsky. Accelerated screening of thermoelectric materials by first-principles computations of electronâĂŞphonon scattering. *Advanced Energy Materials*, 8(20):1800246, 2018.

[14] Gaston Kané, Michele Lazzeri, and Francesco Mauri. Zener tunneling in the electrical transport of quasimetallic carbon nanotubes. *Phys. Rev. B*, 86:155433, Oct 2012.

[15] E. Wigner. On the quantum correction for thermodynamic equilibrium. *Phys. Rev.*, 40:749–759, Jun 1932.

[16] J. E. Moyal. Quantum mechanics as a statistical theory. *Math. Proc. Camb. Philos. Soc.*, 45:99–124, 1949.

[17] H.J. Groenewold. On the principles of elementary quantum mechanics. *Physica*, 12(7):405 – 460, 1946.

[18] Michele Simoncelli, Nicola Marzari, and Francesco Mauri. Unified theory of thermal transport in crystals and glasses. *Nature Phys.*, 15:809–813, 2019.

[19] Rita Claudia Iotti, Fabrizio Dolcini, and Fausto Rossi. Wigner-function formalism applied to semiconductor quantum devices: Need for nonlocal scattering models. *Phys. Rev. B*, 96:115420, Sep 2017.

[20] Z. Zhan, E. Colomés, and X. Oriols. Unphysical features in the application of the boltzmann collision operator in the time-dependent modeling of quantum transport. *J. Comput. Electron.*, 15(4):1206–1218, Dec 2016.

[21] M. Nedjalkov, S. Selberherr, D.K. Ferry, D. Vasileska, P. Dollfus, D. Querlioz, I. Dimov, and P. Schwaha. Physical scales in the wignerâĂŞboltzmann equation. *Ann. Phys.*, 328:220 – 237, 2013.

[22] M. Nedjalkov, D. Querlioz, P. Dollfus, and H. Kosina. *Wigner Function Approach*, pages 289–358. Springer New York, New York, NY, 2011.

[23] Fausto Rossi and Tilmann Kuhn. Theory of ultrafast phenomena in photoexcited semiconductors. *Rev. Mod. Phys.*, 74:895–950, Aug 2002.

[24] R. Hübner and R. Graham. Landau-zener transitions and dissipation in a mesoscopic ring. *Phys. Rev. B*, 53:4870–4885, Feb 1996.

[25] J. B. Krieger and G. J. Iafrate. Quantum transport for bloch electrons in a spatially homogeneous electric field. *Phys. Rev. B*, 35:9644–9658, Jun 1987.

[26] Gaston Kané, Michele Lazzeri, and Francesco Mauri. High-field transport in graphene: the impact of zener tunneling. *J. Phys.: Condends. Matter*, 27:164205, 2015.

[27] Paolo Giannozzi, Stefano Baroni, Nicola Bonini, Matteo Calandra, Roberto Car, Carlo Cavazzoni, Davide Ceresoli, Guido L Chiarotti, Matteo Cococcioni, Ismaila Dabo, Andrea Dal Corso, Stefano de Gironcoli, Stefano Fabris, Guido Fratesi, Ralph Gebauer, Uwe Gerstmann, Christos Gougoussis, Anton Kokalj, Michele Lazzeri, Layla Martin-Samos, Nicola Marzari, Francesco Mauri, Riccardo Mazzarello, Stefano Paolini, Alfredo Pasquarello, Lorenzo Paulatto, Carlo Sbraccia, Sandro Scandolo, Gabriele Sclauzero, Ari P Seitsonen, Alexander Smogunov, Paolo Umari, and Renata M Wentzcovitch. QUANTUM ESPRESSO: a modular and open-source software project for quantum simulations of materials. *J. Phys. Condens. Matter*, 21(39):395502, 2009.

[28] P Giannozzi, O Andreussi, T Brumme, O Bunau, M Buongiorno Nardelli, M Calandra, R Car, C Cavazzoni, D Ceresoli, M Cococcioni, N Colonna, I Carnimeo, A Dal Corso, S de Gironcoli, P Delugas, R A DiStasio Jr, A Ferretti, A Floris, G Fratesi, G Fugallo, R Gebauer, U Gerstmann, F Giustino, T Gorni, J Jia, M Kawamura, H-Y Ko, A Kokalj, E Küçükbenli, M Lazzeri, M Marsili,

N Marzari, F Mauri, N. L. Nguyen, H. V. Nguyen, A Otero de-la Roza, L Paulatto, S Poncé, D Rocca, R Sabatini, B Santra, M Schlipf, A P Seitsonen, A Smogunov, I Timrov, T Thonhauser, P Umari, N Vast, X Wu, and S Baroni. Advanced capabilities for materials modelling with Quantum ESPRESSO. *J. Phys. Condens. Matter*, 29(46):465901, 2017.

[29] Stefano Baroni, Stefano de Gironcoli, Andrea Dal Corso, and Paolo Giannozzi. Phonons and related crystal properties from density-functional perturbation theory. *Rev. Mod. Phys.*, 73:515–562, Jul 2001.

[30] Giovanni Pizzi, Valerio Vitale, Ryotaro Arita, Stefan Blügel, Frank Freimuth, Guillaume Géranton, Marco Gibertini, Dominik Gresch, Charles Johnson, Takashi Koretsune, Julen Ibanez-Azpiroz, Hyungjun Lee, Jae-Mo Lihm, Daniel Marchand, Antimo Marrazzo, Yuriy Mokrousov, Jamal I. Mustafa, Yoshiro Nohara, Yusuke Nomura, Lorenzo Paulatto, Samuel Poncé, Thomas Ponweiser, Junfeng Qiao, Florian Thöle, Stepan S. Tsirkin, MaÅĆgorzata Wierzbowska, Nicola Marzari, David Vanderbilt, Ivo Souza, Arash A. Mostofi, and Jonathan R. Yates. Wannier90 as a community code: new features and applications, 2019.

[31] Atsushi Togo and Isao Tanaka. Spglib: a software library for crystal symmetry search, 2018.

[32] Yoyo Hinuma, Giovanni Pizzi, Yu Kumagai, Fumiyasu Oba, and Isao Tanaka. Band structure diagram paths based on crystallography. *Comput. Mater. Sci.*, 128:140 – 184, 2017.

[33] G. Martinez, B. A. Piot, M. Hakl, M. Potemski, Y. S. Hor, A. Materna, S. G. Strzelecka, A. Hruban, O. Caha, J. Novák, A. Dubroka, C. Drašar, and M. Orlita. Determination of the energy band gap of bi2se3. *Sci. Rep.*, 7:6891, 2017.

[34] John M Ziman. *Electrons and phonons: the theory of transport phenomena in solids*. Oxford university press, 1960.

[35] Hyun-Sik Kim, Zachary M. Gibbs, Yinglu Tang, Heng Wang, and G. Jeffrey Snyder. Characterization of lorenz number with seebeck coefficient measurement. *APL Materials*, 3(4):041506, 2015.

[36] K. C. Lukas, W. S. Liu, G. Joshi, M. Zebarjadi, M. S. Dresselhaus, Z. F. Ren, G. Chen, and C. P. Opeil. Experimental determination of the lorenz number in $cu_0.01bi_2te_2.7se_0.3$ and $bi_0.88sb_0.12$. *Phys. Rev. B*, 85:205410, May 2012.

[37] Yani Chen, Jinlong Ma, and Wu Li. Understanding the thermal conductivity and lorenz number in tungsten from first principles. *Phys. Rev. B*, 99:020305, Jan 2019.

[38] Nicola Marzari, Arash A. Mostofi, Jonathan R. Yates, Ivo Souza, and David Vanderbilt. Maximally localized wannier functions: Theory and applications. *Rev. Mod. Phys.*, 84:1419–1475, Oct 2012.

[39] E. I. Blount. Formalisms of band theory. *Solid State Phys.*, 13:305 – 373, 1962.

[40] Ralph Gebauer and Roberto Car. Kinetic theory of quantum transport at the nanoscale. *Phys. Rev. B*, 70:125324, Sep 2004.

[41] William R. Frensley. Boundary conditions for open quantum systems driven far from equilibrium. *Rev. Mod. Phys.*, 62:745–791, Jul 1990.

[42] Andrea Cepellotti and Nicola Marzari. Thermal transport in crystals as a kinetic theory of relaxons. *Phys. Rev. X*, 6:041013, Oct 2016.

[43] W. H. Jiao, S. Jiang, C. M. Feng, Z. A. Xu, G. H. Cao, M. Xu, D. L. Feng, A. Yamada, K. Matsubayashi, and Y. Uwatoko. Growth and characterization of bi2se3 crystals by chemical vapor transport. *AIP Advances*, 2(2):022148, 2012.

[44] Zhi Ren, A. A. Taskin, Satoshi Sasaki, Kouji Segawa, and Yoichi Ando. Observations of two-dimensional quantum oscillations and ambipolar transport in the topological insulator bi_2se_3 achieved by cd doping. *Phys. Rev. B*, 84:075316, Aug 2011.

[45] James G. Analytis, Ross D. McDonald, Scott C. Riggs, Jiun-Haw Chu, G. S. Boebinger, and Ian R. Fisher. Two-dimensional surface state in the quantum limit of a topological insulator. *Nature Phys.*, 6:960–964, 2010.

[46] Kevin F. Garrity, Joseph W. Bennett, Karin M. Rabe, and David Vanderbilt. Pseudopotentials for high-throughput dft calculations. *Comput. Mater. Sci.*, 81:446 – 452, 2014.

[47] K. Schubert, K. Anderko, M. Kluge, H. Beeskow, M. Ilschner, E. Dörre, and P. Esslinger. Strukturuntersuchung der legierungsphasen cu_2te, cute, cu_3sb, inte, bi_2se_3, pd_5sb_3 und pd_5bi_3. *Naturwissenschaften*, 40:269, 1953.

[48] Jonathan R. Yates, Xinjie Wang, David Vanderbilt, and Ivo Souza. Spectral and fermi surface properties from wannier interpolation. *Phys. Rev. B*, 75:195121, May 2007.